Acta of Bioengineering and Biomechanics
Vol. 23, No. 1, 2021

Original paper
DOI: 10.37190/ABB-01749-2020-03

Numerical analysis of the biomechanical effects on micro-vessels by ultrasound-driven cavitation

WENYI LIU, JIWEN HU*, YATAO LIU, WEIRUI LEI, XUEKUN CHEN

College of Mathematics and Physics, University of South China, Hengyang, China.

Purpose: The goal of this study was to evaluate the biomechanical effects such as sonoporation or permeability, produced by ultrasound-driven microbubbles (UDM) within microvessels with various parameters. *Methods*: In this study, a bubble-fluid-solid coupling system was established through combination of finite element method. The stress, strain and permeability of the vessel wall were theoretically simulated for different ultrasound frequencies, vessel radius and vessel thickness. *Results*: the bubble oscillation induces the vessel wall dilation and invagination under a pressure of 0.1 MPa. The stress distribution over the microvessel wall was heterogeneous and the maximum value of the midpoint on the inner vessel wall could reach 0.7 MPa as a frequency ranges from 1 to 3 MHz, and a vessel radius and an initial microbubble radius fall within the range of 3.5–13 μm and 1–4 μm, respectively. With the same conditions, the maximum shear stress was equal to 1.2 kPa and occurred at a distance of ±5 μm from the midpoint of 10 μm and the maximum value of permeability was 3.033×10^{-13}. *Conclusions*: Results of the study revealed a strong dependence of biomechanical effects on the excitation frequency, initial bubble radius, and vessel radius. Numerical simulations could provide insight into understanding the mechanism behind bubble-vessel interactions by UDM, which may explore the potential for further improvements to medical applications.

Key words: *ultrasound, cavitation, stress, strain, permeability*

1. Introduction

Ultrasound-driven microbubbles (UDM) have gained special attention due to their application in ultrasound imaging and therapy [4]. Microbubbles, when confined in the blood stream, remain intravascular and undergo a volumetric oscillation when activated by an ultrasound. A number of studies have shown that microbubbles could induce mechanical bioeffects on their confining vessels [7], [17], [20]. The effects could be therapeutically beneficial and might range from increasing the vascular permeability for intravascular local drug and gene delivery, opening the blood–brain barrier (BBB) locally and transiently to vessel rupture and occlusion [25]. One major challenge in using microbubbles for medical ultrasound application is the lack of knowledge about the behavior of confined bubbles and the impact bubbles might have on the surrounding tissue.

Besides experimental reports, several numerical models were also developed to depict the dynamics of bubbles confined inside blood vessels. For instance, Sassaroli and Hynynen [24] developed a two-dimensional (2D) model to simulate a rectangular bubble oscillating in a rigid vessel. Ye and Bull presented a 2D boundary element model (BEM) to simulate the asymmetric expansion of a free-gas bubble in both rigid and flexible vessels including an inviscid fluid [29]. Using a lumped-parameter model that took the bubble shell and the fluid viscosity into account, Qin and Ferrara investigated the natural frequency of nonlinear oscillations of UCAs in a partially compliant and stiffness vessels [21]. In addition, many asymmetric models were proposed to simulate the asymmetric oscillations and acoustic responses of the bubble in a small vessel,

* Corresponding author: Jiwen Hu, Jiwen Hu, College of Mathematics and Physics, University of South China. E-mail: hu_sanping@163.com

Received: November 2nd, 2020
Accepted for publication: January 18th, 2021

based on the boundary element method (BEM), the finite element method (FEM) or the combination of these two methods [16], [7], [13]. These numerical results predicted that vascular damage could occur during vascular injections due to the elevated wall shear stress and circumferential stress.

It is generally accepted that the expansion and contraction of encapsulated microbubbles in an ultrasound field induces microstreaming in the surrounding fluid. If cells are present near oscillating microbubble, microstreaming-induced shear stress may cause biological effects on neighboring cells [30]. The shear stress related to micro-streaming was relatively high compared to the shear stress associated with blood flow (0.1–4 Pa). Consequently, these UDMs induced elevated shear stress levels maybe greatly enhance the permeability of blood vessel wall. Several models have been proposed for the microbubble-cell interaction in sonoporation focusing on different aspects: cell expansion and microbubble jet velocity [28], the shear stress exerted on the cell membrane [30], microstreaming of the shear stress exerted on the cell membrane in combination with microstreaming [13] generated by an oscillating microbubble. In contrast to the other models, Man et al. [15] proposed that microbubble-generated shear stress does not induce pore formation, but is, instead, the results of microbubble fusion with the membrane and subsequent "pull out" of cell membrane lipid molecules by the oscillating microbubble. Models for pore formation and resealing in cell membranes have also been developed, but these models neglected the mechanism by which the pore was created. If the shear stress is high enough, it may have an impact on the cell membrane integrity or even detachment of the endothelial cells. Normal stress, the other important stresses, might be responsible for vessel rupture. Vascular rupture caused by the bubble activity was observed and reported in different studies [2], [7].

Despite the great potential of permeability/sonoporation as a promising drug delivery technique in medicine, its applications have been limited mostly by the lack of understanding the underlying biophysical mechanism, especially, many aspects of the mechanical mechanisms involved in the UDM stress in action in permeability have not yet been fully understood. The current study aims to simulate non-spherical oscillation of a microbubble inside a microvessel and provide a comprehensive analysis regarding the biomechanical effects of the varying acoustic frequency, vessel size and initial bubble radii by using finite element method. The paper focused on the calculation of the stress and strain, especially, the permeability of endothelial vessel wall.

2. Theory

2.1. Analytical microbubble model in an elastic microvessel

The 2D geometry of the bubble-blood-vessel system was schematically illustrated in Fig. 1, where the microbubble was located in the center of the microvessel, L is length of the vessel, d is the thickness of the vessel wall, R_T is the initial radius of the vessel. The origin of the cylindrical coordinate system is at the bubble's center, the radial coordinate is orthogonal to the vessel wall and the axial coordinate is parallel to the vessel wall.

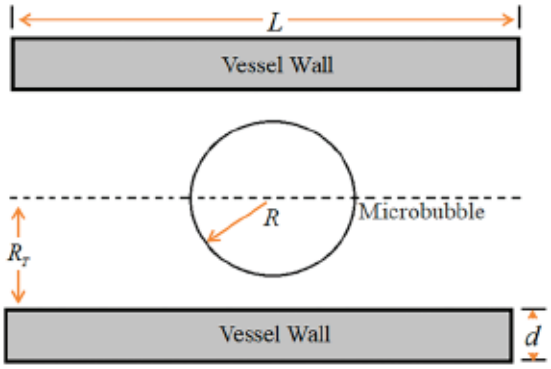

Fig. 1. Microvesicle-blood-vessel wall coupling model

The physics of a single microbubble oscillating in a microvessel filled with viscous fluid can be characterized as follows [9]:

$$R\ddot{R}\left(1+\frac{R}{R_T}\left(\frac{L}{R_T}+0.224\right)\right)$$
$$+1.5\dot{R}^2\left(1+\frac{4R}{3R_T}\left(\frac{L}{R_T}+0.224\right)\right)=\frac{\Delta P}{\rho}, \qquad (1)$$

where R refers to radius as a function of time, a dot represents a time-derivative, ρ is the density of the fluid, and ΔP is the difference in pressure between the bubble wall and infinity. ΔP can take many forms depending on the conditions, damping, shell parameters, etc. A common expression is:

$$\Delta P=\left(P_0-P_V+\frac{2\sigma}{R_0}\right)\left(\frac{R_0}{R}\right)^{3\gamma}$$
$$-\frac{2\sigma}{R}-4\mu\frac{\dot{R}}{R}+P_V-P_0-P_a\sin(\omega t), \qquad (2)$$

where R_0 is the equilibrium radius of the bubble, P_0 is the ambient pressure, P_v is the vapor pressure, σ is the surface tension, η is the viscosity, P_a is the applied acoustic pressure, ω is the driving frequency, t is the time, and γ is the polytropic exponent, also known as the ratio of specific heats.

2.2. Blood fluid model

Assuming that the blood is an incompressible fluid, the Navier–Stokes equation is used to model the blood [22]:

$$\nabla \cdot \vec{u} = 0, \tag{3}$$

$$\rho\left(\frac{\partial \vec{u}}{\partial t} + (\vec{u} \cdot \nabla)\vec{u}\right) + \nabla \cdot (-pI + \mu(\nabla \vec{u} + \nabla u^T)) = 0, \tag{4}$$

where ρ and μ are respectively the blood density and dynamic, I and u are the unit tensor and velocity of flow.

2.3. Vessel wall model

Assuming that the vessel wall is a homogeneous isotropic linear elastic material, and ignoring its volume force, the dynamic process of the displacement of the vessel wall with time deformation can be expressed by the following equation:

$$(\lambda + \mu)\frac{\partial^2 \vec{\upsilon}_j}{\partial x_j \partial x_i} + \mu \frac{\partial^2 \vec{\upsilon}_i}{\partial x_j \partial x_j} = \rho_w \frac{\partial^2 \vec{\upsilon}_i}{\partial t^2}, \tag{5}$$

where ρ_W and $\vec{\upsilon}$ are vessel wall density and vessel wall displacement; λ and μ are Lamè constant; the values in this paper are 1.59 MPa and 1.03 kPa. According to the principle of mechanics, the strain and displacement of vessel wall, strain and stress are related as follows:

$$\varepsilon_{ij} = \frac{1}{2}(\upsilon_{i,j} + \upsilon_{j,i}), \tag{6}$$

$$\sigma_{ij} = \frac{E}{1+\nu}\left(\varepsilon_{ij} + \frac{\nu}{1-2\nu}\varepsilon_{kk}\delta_{ij}\right), \tag{7}$$

where E and v are Young's modulus and Poisson's ratio of the vessel wall respectively; σ_{ij}, ε_{ij} are stress component and strain component respectively. When $i = j$, δ_{ij} is equal to 1; when $i \neq j$, δ_{ij} is equal to 0.

2.4. Boundary conditions

Two interaction boundaries between bubble-fluid and fluid-solid should be constructed in bubble-fluid-solid model. In the bubble-fluid interaction, the conservation of mass and momentum is satisfied, and the corresponding dynamic equation can be expressed as:

$$\frac{\partial \rho}{\partial t} + \nabla \cdot (\rho \vec{u}) = 0, \tag{8}$$

$$\rho\left(\frac{\partial \vec{u}}{\partial t} + (\vec{u} \cdot \nabla)\vec{u}\right) = \nabla \cdot (-pI + \mu(\nabla \vec{u} + \nabla u^T)), \tag{9}$$

where $\vec{u}$ is the fluid velocity of the microbubble wall, according to the principle of continuity, the radial velocity of the bubble oscillation is equal to the velocity of the adjacent fluid, $\dot{R} = \vec{u}$. Similarly, in the process of blood and vessel wall action, the continuity of velocity and force is satisfied, namely, the following equation can be obtained:

$$u = \frac{\partial \vec{\upsilon}_s}{\partial t}, \tag{10}$$

$$\sigma \cdot n = (-pI + \mu(\nabla \vec{u} + (\nabla \vec{u})^T)) \cdot n, \tag{11}$$

where $\vec{\upsilon}_s$ and n are the vibration velocity of the vessel wall and the unit normal phase vector, respectively.

2.5. Permeability of vessel wall

The microbubble vibration under ultrasonic field produces shear force on the inner wall of blood vessels. Based on the results of clinical experiments, the relation of the shape index (SI) was found that [14]:

$$SI = 0.38 \times e^{-0.79 \cdot \tau} + 0.225 \times e^{-0.043 \cdot \tau}. \tag{12}$$

The shape index was associated with the number of mitotic cells per area of 0.64 mm^2. The function fitted by Olgac et al. to the data from [19] takes the following form:

$$N_{MC} = 0.003797 \times e^{-14.75 \cdot SI}. \tag{13}$$

On the basis of the work [14], the correlation of the number of mitotic cells with the number of all leaky junctions per area of 0.64 mm^2 was derived. It was assumed that the number of leaky cells correlated with nonmitotic cells is independent on τ. This relation is the following:

$$N_{LC} = 0.307 + 0.805 \times N_{MC}. \tag{14}$$

The number of leaky cells in a given area fraction of leaky junctions was determined to be:

$$\phi = \frac{N_{LC} \times \pi R_{cell}^2}{6.4 \times 10^{-7}}, \quad (15)$$

where R_{cell} is the radius of the endothelial cell taken as 15 μm. The endothelium permeability K_{end} can be expressed as a sum of permeabilities of parallel pathways [14]:

$$K_{end} = K_{lj} + K_{nj}. \quad (16)$$

The permeability of the leaky junctions K_{lj} is dependent on the fraction of leaky junction ϕ and may be determined using formula for the permeability of a list of width $2w$ mutiplied by area fraction of a leaky junctions:

$$K_{lj} = \frac{4w^3\phi}{3R_{cwll}}, \quad (17)$$

where w is the leaky junction of half-width taken as 10 nm. The shear stress does not affect the normal junctions, so K_{nj} is a constant. Therefore, it can be determined by using known data for K_{lj} ($\phi = 5e - 4$) $= 3.22e - 15$ mm^2, thus [14]:

$$K_{nj} = K_{end}(\phi = 5 \times 10^{-4}) - K_{lj}(\phi = 5 \times 10^{-4}). \quad (18)$$

Table 1. Values of parameters in this study [21]

Name	Parameter	Value [unit]
Gas polytropic	γ	1.07
Saturated vapor pressure	P_V	2330 [Pa]
The initial radius of the microbubble	R_0	2 [μm]
Gas-liquid surface tension	σ	0.056 [N/m.]
The density of blood	ρ	1059 [kg/m^3]
Sound pressure	P_a	0.1–0.2 [MPa]
Hemodynamic viscosity	μ	0.0035 [Pa·s]
Blood vessel density	ρ_w	1000 [kg/m^3]
Young's modulus of blood vessel	E	3.0 [MPa]
Vascular Poisson's ratio	ν	0.49

2.6. Description of the simulation

Based on low-intensity ultrasonic pressure, the interaction between the microbubble oscillation and the blood vessel wall surface during steady-state cavitation was studied, and the model was shown in Fig. 1. The length of the microvessel in the whole study is L = 200 μm. According to the distribution characteristics of the stress and force, the relative microbubble scale can be regarded as infinite. Ignoring the influence of the length of the blood vessel, we intercepted the 20 μm near the microbubble for analyzing. The simulation parameters are described in Table 1. Equations of bubble-fluid-wall interaction with initial and boundary conditions are solved by utilizing the finite element method (FEM) via COMSOL Multiphysics 5.3 (Comsol, Inc.; Burlington, MA). In the model depicted in Fig. 1, unit size free triangle mesh is used to partition the model. A maximum mesh size of $\lambda/6$ (λ is the wavelength) in the focal region and a maximum mesh size of $\lambda/4$ in the rest of the domain is used for grid generation. The vessel walls are consisted of 5086 vertices of mesh and 9570 triangular elements, and the plaque is built of 710 vertices and 1208 triangular elements. In addition, the blood contains 4937 vertices and 9570 triangular units. For details on the simulation process, see the supplementary materials.

3. Results

In this manuscript, we focused on the effect of each dynamic tissue property independent from each other, and compared these effects with the conventional method of keeping the tissue properties constant. When the effect of one dynamic tissue property was studied, the other tissue properties remained constant unless otherwise noted. In the following study, the amplitude of acoustic pressure on the sound source face P_a is 1×10^5 Pa unless otherwise noted.

3.1. Mechanical effect of ultrasonic frequency

In Figure 2, the micro-jet velocity profile and the maximum stress response of circumferential stress (CS) at different frequencies for R_T = 8 μm and R_0 = 2 μm was shown. Among the three frequencies chosen here, CS peaks reached about 0.7, 0.13 and 0.053 MPa, respectively. The maximum CS calculated for f = 1.0 MHz exceeded the minimum reported vascular strength [2], [21]. This suggested that the bubble might have ruptured the vessel wall to some extent. The simulation results agreed with previous research findings [1], [2]. In Figure 2, the micro-jet velocity peaked at the three frequencies are 2.26, 0.92 and 0.63 m/s, respectively. The peak velocity at 1 MHz was almost 4 times that of 3 MHz. It is manifested that the influences of driving frequency on CS and micro-jet velocity was quite remarkable.

In Figure 3, the curve variation of the normal stress of vessel wall at different time under three frequency drives was shown. Here, the positive and negative normal stresses corresponded to bubble expansion and compression phases respectively. The peak values of normal stress for expansion and contraction were 59.6 kPa and 15.4 kPa at a frequency of 1.0 MHz, and decrease with increasing frequency. This suggests that the wall oscillation weakens, which does less harm to the vessel, as increased the driving frequency due to normal stresses.

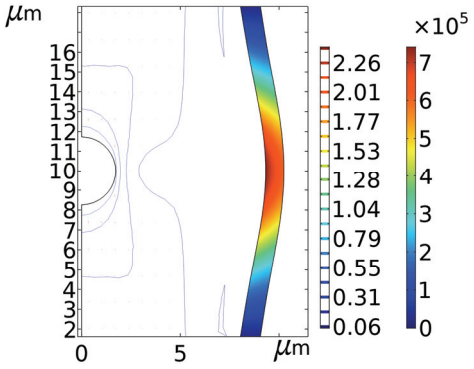

(a) f = 1 MHz

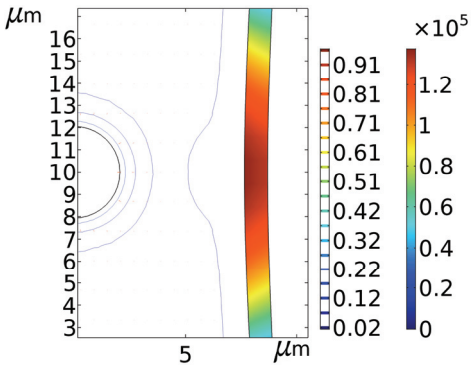

(b) f = 2 MHz

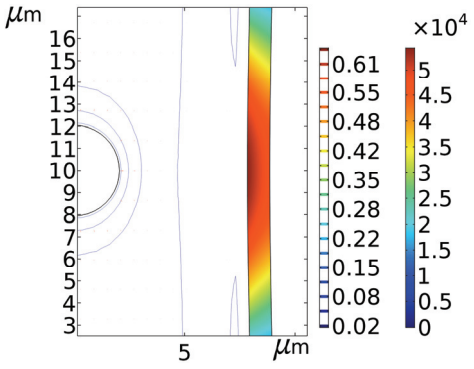

(c) f = 3 MHz

Fig. 2. Profiles of maximum stress of vessel wall at different ultrasonic frequencies

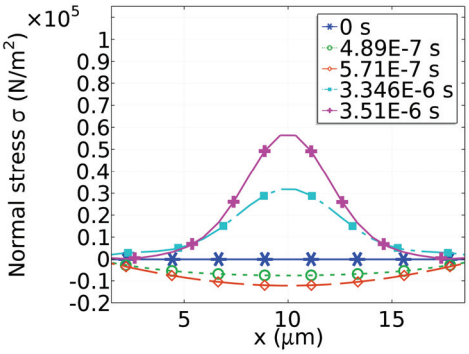

(a) f = 1 MHz

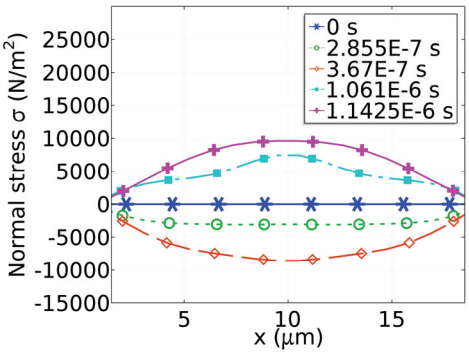

(b) f = 2 MHz

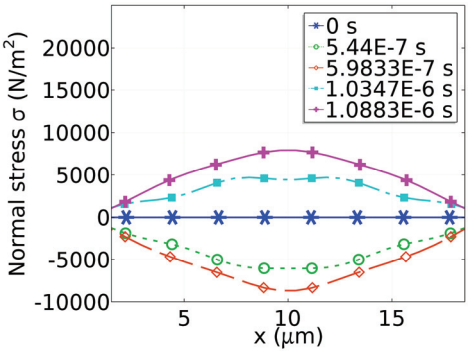

(c) f = 3 MHz

Fig. 3. Variation curves of the normal stress on vessel wall at different frequencies

The results depicted in Figure 4 show that the maximum shear stresses of wall are position and frequency-dependent. Unlike the NS case, the shear stress peaks occurr near x = 5 μm and 15 μm, and are 1.2, 0.21 and 0.18 kPa, respectively. For a bubble (2.0 μm in radius) activated by 1 – MHz ultrasound pulses in a microvessel with a radius of 5.0 μm can be generated on the vessel wall at a driving pressure of 0.2 MPa, which should be high enough to damage the vascular endothelial cells [18]. Comparing Figs. 4 and 5 show the similar change of the maximum permeability distribution induced by shear stress. The peak

permeability at 1.0 MHz was 3.032×10^{-13}. A low-frequency UDM could increase vascular permeability and result in convective extravasation of a macromolecule drug [27].

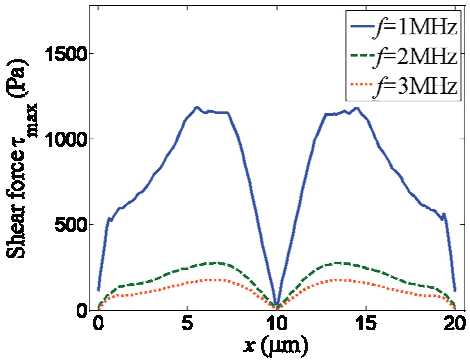

Fig. 4. The maximum shear stress of the vessel wall under different ultrasonic frequencies

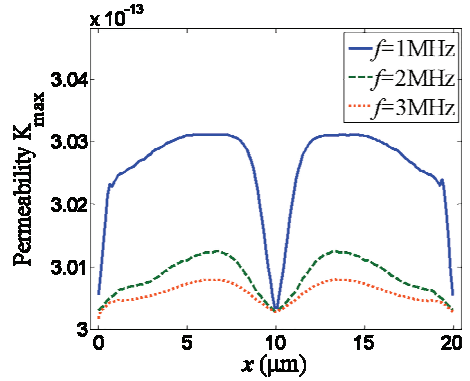

Fig. 5. The maximum permeability of vessel wall at different ultrasonic frequencies

3.2. Effect of vessel diameter

In Figure 6, the maximum stress response at different snapshots in time for three vessel radii with a driving frequency f = 1 MHz and an initial radius R_0 = 2 μm is shown. The peak stresses are 26.3, 17.5 and 15.1 kPa when the vessel radii are 6, 10 and 12 μm, respectively, but as seen in Fig. 6, the maximum normal stress happens in compression phases of bubble oscillation. In some cases, vessel invagination may play a more important role than distention in causing vessel rupture, as it may generate higher strains on the vessel wall than distention [1]. In Figure 7, the maximum shear stress distribution is illustrated. It can be noted that the shear stress peaks drift away the center when increasing the distance of bubble and wall. A similar result was also obtained or observed in papers [8], [12]. In addition to frequency, the vessel size has a significant influence on the maximum permeability distribution as shown in Fig. 7. For instance, the maximum permeability as a function of vessel radius for f = 1 MHz could be seen in Fig. 8. This curve peaks at R_T = 6.7 μm suggesting that 1.0 MHz was the resonance frequency of 2 μm bubbles.

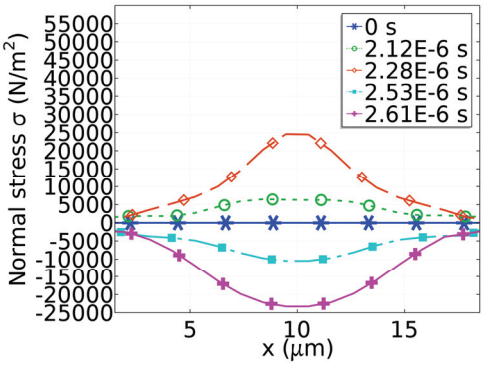

(a) R_T = 6 μm

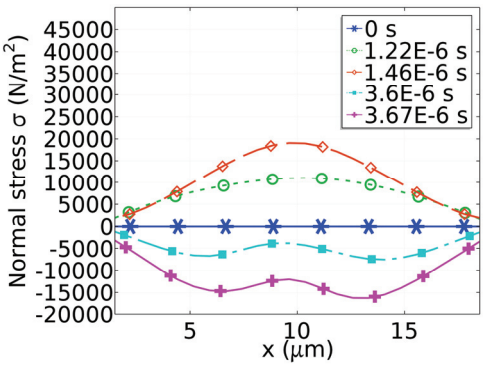

(b) R_T = 10 μm

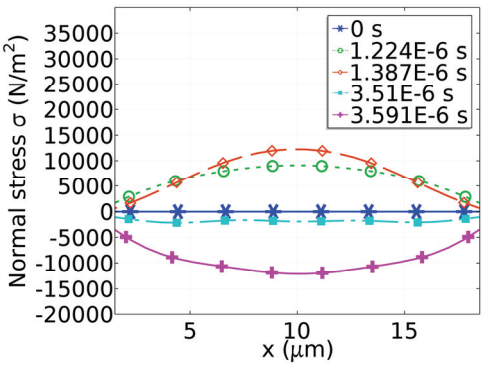

(c) R_T = 12 μm

Fig. 6. Normal stress of vessel wall for different vessel radii at different times

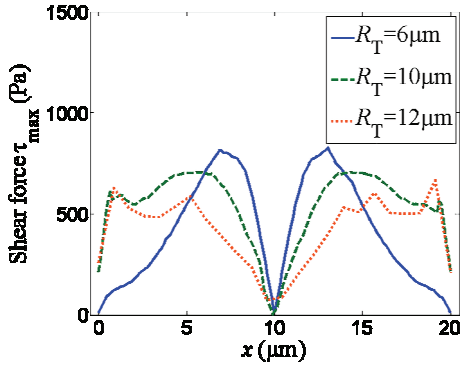

Fig. 7. The maximum shear stress of the vessel wall at different vessel radii

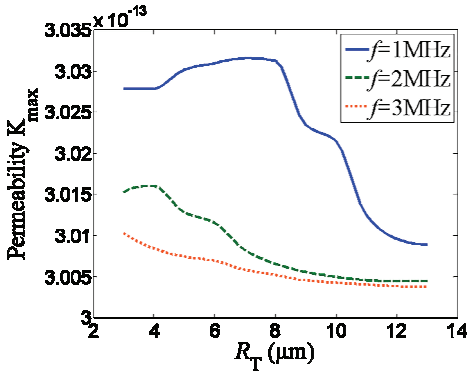

Fig. 8. The maximum permeability of the vessel wall at different blood vessels

3.3. Effect of the initial microbubble radius

To further study bubble-vessel interactions, the initial radii of bubbles ranging from 0.5 to 5.0 μm on shear stress were examined. Compared to stress in Figs. 4–6, in Figs. 9 and 10, the similar changes of the maximum normal and shear stresses for f = 1 MHz and R_T = 8.0 μm are shown. However, the microbubble sizes have important influence on the mechanical effects to the vessel wall, as shown in Fig. 9. It was previously shown that the extent of BBB opening varied with bubble size [3]. The authors reported the calculated stress from bubbles of 4–5 μm exert larger wall stresses compared to 1–2 μm bubbles as bubbles confined within the blood vessel with a radius of 6 μm. The stresses in Figure 9 have the similar tendency as in experimental observation and simulation [3]. On the other hand, it can be seen in Fig. 11 that the greater the frequency, the greater the impact on the permeability of the blood vessel wall. Under the three frequencies, as the radius of the microbubble expanded, the permeability first increased and then decreased. The simulations indicate the optimization of the ultrasound frequency, and bubble size for maximum BBB opening.

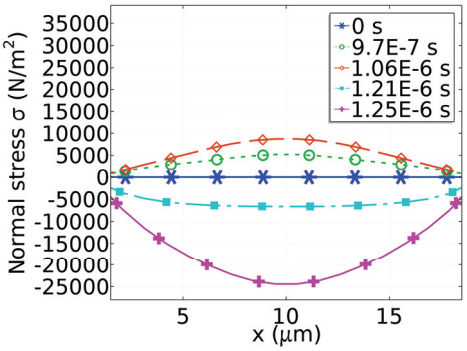

(a) R_0 = 1 μm

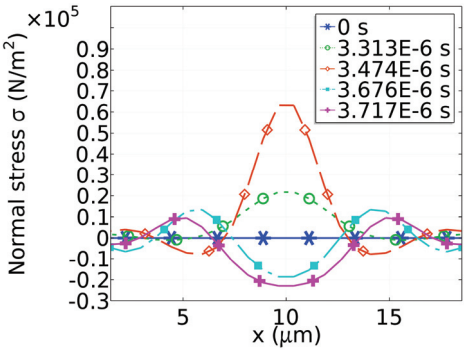

(b) R_0 = 3 μm

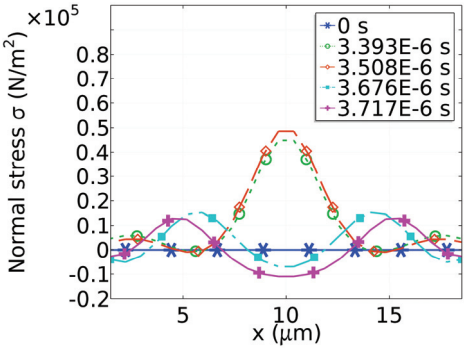

(c) R_0 = 4 μm

Fig. 9. Normal stress curves of vessel wall for different initial microbubble radii at different times

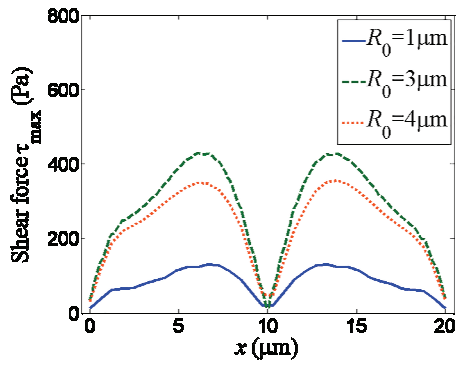

Fig. 10. The maximum shear force on vessel wall for different microbubble initial radii

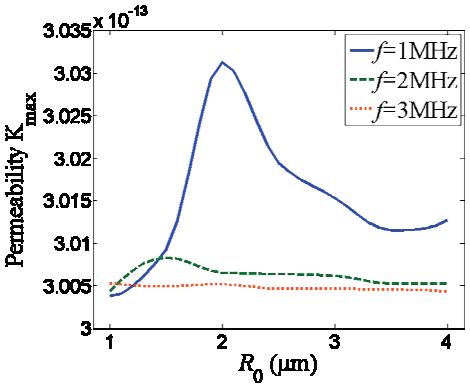

Fig. 11. The maximum permeability of the vessel wall for different initial microbubble radii at three ultrasound frequencies

4. Discussion

In this study, a finite element model of a coupled bubble/fluid/vessel system was developed and provided a means to predict which mechanism was responsible for UDM bioeffects. The numerical simulation was performed using an axisymmetrical assumption. The bubble model took the radius R_T and the length L of microvessel into account. When microvessel diameters were comparable to bubble sizes at relatively low acoustic pressures (100–200 kPa), the simulation results could converge to the results of previous models [1], [2], [7]. As shown in Fig. 3, the vessel wall vibrations experienced a transition from nonlinear to linear oscillations when the driving pressures was 0.1 MPa and the driving frequency increased from 1 MHz to 3 MHz. The displacement patterns of the vessel wall, as illustrated in Fig. 2, changed with time and were associated with the frequency [6], [21], [28]. UDM at relatively low frequencies could increase vascular permeability [26]. Meanwhile, we demonstrated the stresses patterns of the entire vessel wall, not just a specified point of vessel wall [7], [13]. On the other hand, we focused on the vessel stresses for different initial bubble radii and frequencies, as shown in Fig. 13, which were important for the shear intensity [18], and vessel sonoporation/permeability [27]. Increasing the pressure to 0.2 MPa, the wall deformation increased dramatically, as shown in Fig. 12. Schematics from figures 2 and 12 showed that the maximum CS values were between 0.04–1.1 MPa during bubble expansion and 0.1–3.6 MPa during bubble shrinkage. Shear stresses were between 0.13–1.2 kPa during expansion and 0.18–1.6 kPa were injected, as shown in Figs. 4, 7 and 10. These results confirmed that vessel damage could occur during vascular injections [1], [7].

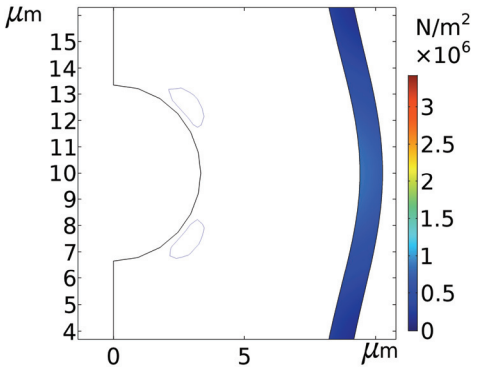

(a) Vessel distention

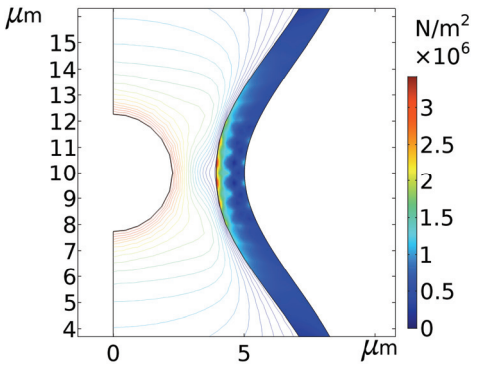

(b) Vessel invagination

Fig. 12. Profiles of maximum stress of vessel wall for $R_0 = 2$ μm and $R_T = 8$ μm

UDM could produce liquid jets and local shear stress that could alter biological membranes and facilitate drug transport [21], [28], [30], but there was no consensus as to whether inertial or non-inertial cavitation played the most important role in sonoporation [15], and regarding the biophysical mechanisms of sonoporation: microbubble jet velocity [5], shear stress [28], the shear stress in combination with microstreaming [8], [28], [30]. In our simulations as seen in Figs. 4, 7 and 10, the shear stresses showed a V-shaped curve, the substantial shear stress on the surface occurs inside a circular zone with a radius about two-thirds of the bubble radius [8], [11]. The permeability distribution, as shown in Figs. 5 and 13, experienced almost the same changes as the shear stress did. It suggested that the microstreaming-shear stress was an important factor in sonoporation/permeability [12], [30]. Moreover, direct optical evidence demonstrated that microstreaming generated by a stably oscillating bubbles can entrain approaching lipid vesicles and later tear them up due to the high shear stresses induced [4]. It was noted that the wall permeability

tended to be constant once the shear stress reached a critical value, which was computed by a fitting function from experimental data. A possible explanations was that there were the largest pores generated by shear stress, as specified by Eqs. (12) and (13), [19], which might protect the endothelium against apoptosis and rupture. Interestingly, there was no significant difference in the permeability seen in Fig. 13 during the vessel's expansion and contraction phases. Figure 13 indicated

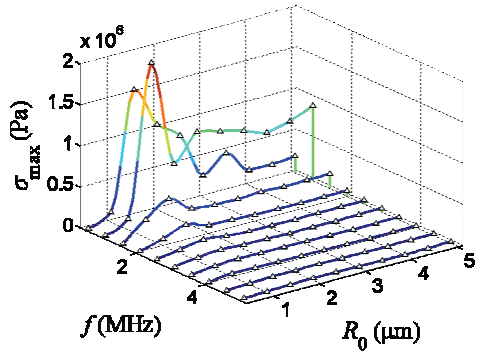

Fig. 13. Stress response curve for the bubble vibration as a function of initial bubble radius and driving frequency during the bubble expansion for R_T = 8 μm

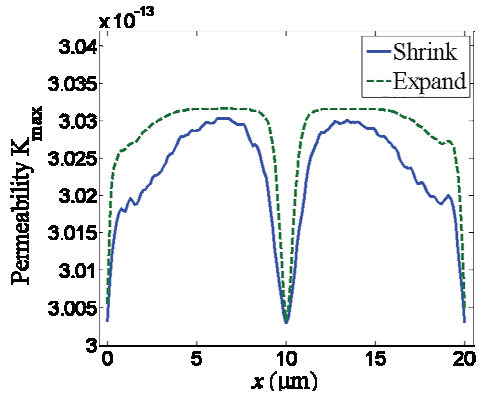

(a) R_0 = 2 μm

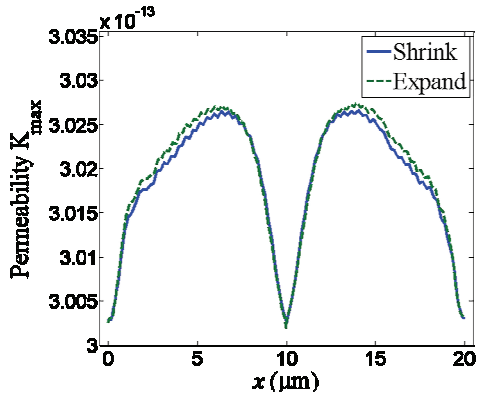

(b) R_0 = 4 μm

Fig. 14. The maximum permeability of the vessel wall for R_0 = 4 μm and P_a = 0.2 MPa

that sonoporation/permeability was not significantly affected by the normal stress. This estimate was consistent with the result of experiment that have investigate the sonoporation occurrence [6].

Significant efforts have been made to model the UDM dynamics [13], [36], [21]. Various independent investigations indicate that the presence of microbubbles within blood vessels may increase the likelihood of ultrasound-induced damage [16]. However, previous studies focused primarily on the morphological evolution of a microbubble [13] and the deformations of the vessel wall induced by UDM [16], [13] within a constrained vessel, less attention has been paid to the study of the stress and strain fields of the vessel wall [13], especially the sonoporation of vessel wall [28]. As expected, the maximum tube dilation and maximum hoop stress were found to occur well before the bubble reached its maximum radius [16]. As the wall thickness, vessel radius, and acoustic frequency decreased, the maximum hoop stress increased, indicating a higher potential for tube rupture and hemorrhage [16]. In contrast to the other models, we focused on the spatial distribution of endothelial permeability produced by shear stress on the deformed vessel wall, which has important influence on sonoporation [14], [28]. In addition, several models have been proposed for the microbubble-cell interaction in sonoporation focusing on a oscillating microbubble near a rigid plane with semi-analytical method [16], [28], Boundary Element Method (BEM) [12]. Compared to the reports mentioned above, our model explores more in-depth study of the nonlinear dynamic characteristics of blood vessels and the distribution of permeability with a time-dependent shear stress by UDM.

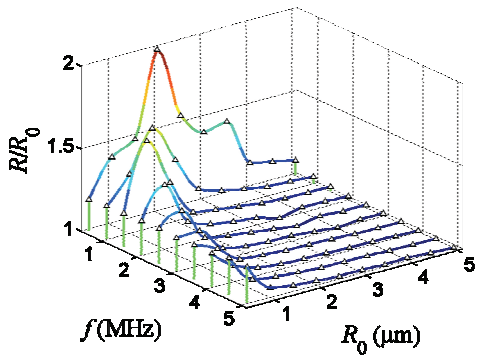

Fig. 15. Amplitude response curve for the bubble vibration as a function of initial bubble radius and driving frequency during the bubble expansion for R_T = 8 μm

As shown in Figs. 13 and 15, the stress on the vessel wall is positively correlated to the amplitude. For safe and effective application of UDM for enhanc-

ing vessel permeability, opening of the blood–brain barrier and increased transdermal drug delivery with sonoporation [25], an ultrasound wave must be combined with the vessel size, initial bubble radius and driving frequency, and further refinement in the optimal parameters for avoiding vessel hemorrhage. There were, of course, still some improvements to the current model. For example, the model did not take the bubble shell materials and the wall microstructural arrangement into account [22], and the bubble fracture process itself was not modelled in this study.

5. Conclusions

In this paper, based on clinical microvascular data and using the principle of hemodynamics, we have developed a novel computational framework combining fluid–structure coupling and interface tracking to model the nonlinear dynamics of the vessel wall in constrained environments. The interaction between an UDM and vessel wall was calculated using the finite element method. The mechanical forces from UDM not only caused vessel wall deformation, but also triggered "good" or "harmful" effects on the vessel wall. The biomechanical effects were affected by driving frequency, vessel diameter, and initial bubble radius. It was noted that the sonoporation/permeability of vessel wall was most affected by the shear stress. This paper gave a detailed understanding of the biomechanical effects under UMD and might enable one to explore a wide range of parameters to identify promising experimental and practical configurations and setups and to help optimize permeability for achieving increased drug uptake with minimum wall damage.

Acknowledgements

This study was carried out with financial support from the National Natural Science Foundation of China [11747121, 11904161], the Natural Science Foundation of Hunan Province of China [13JJ3076] and the key scientific research project of the Department of Education of Hunan Province [14A127].

References

[1] CHEN H., BRAYMAN A.A., BAILEY M.R., MATULA T.J., *Blood vessel rupture by cavitation*, Urol. Res., 2010, 38 (4), 321–326, DOI: 10.1007/s00240-010-0302-5.

[2] CHEN H., KREIDER W., BRAYMAN A.A., BAILEY M.R., MATULA T.J., *Blood vessel deformations on microsecond time scales by ultrasonic cavitation*, Phys. Rev. Lett., 2011, 106 (3), 034301, DOI: 10.1103/PhysRevLett.106.034301.

[3] CHOI J.J., FESHITAN J.A., BASERI B., WANG S., TUNG Y.S., BORDEN M.A., KONOFAGOU E.E., *Microbubble-size dependence of focused ultrasound-induced blood-brain barrier opening in mice in vivo*, IEEE. Trans. Biomed. Eng., 2010, 57 (1), 145–154, DOI: 10.1109/TBME.2009.2034533.

[4] FAN Z., KUMON R.E., DENG C.X., *Mechanisms of microbubble-facilitated sonoporation for drug and gene delivery*, Ther. Deliv., 2014, 5 (4), 467–486, DOI: 10.4155/tde.14.10.

[5] GUO X., CAI C., XU G., YANG Y., TU J., HUANG P., ZHANG D., *Interaction between cavitation microbubble and cell: A simulation of sonoporation using boundary element method (BEM)*, Ultrason. Sonochem., 2017, 39, 863–871, DOI: 10.1016/j.ultsonch.2017.06.016.

[6] HELFIELD B., CHEN X., WATKINS S.C., VILLANUEVA R.S., *Biophysical insight into mechanisms of sonoporation*, Proc. Natl. Acad. Sci., 2016, 113 (36), 9983–9988, DOI: 10.1073/pnas.1606915113.

[7] HOSSEINKHAH N., CHEN H., MATULA T.J., BURNS P.N., HYNYNEN K., *Mechanisms of microbubble-vessel interactions and induced stresses: a numerical study*, J. Acoust. Soc. Am., 2013, 134 (3), 1875–1885, DOI: 10.1121/1.4817843.

[8] HU J.W., QIAN S.Y., SUN J.N., LÜ Y.B., HU P., *Microflow-induced shear stress on biomaterial wall by ultrasound-induced encapsulated microbubble oscillation*, Chin. Phys. B., 2015, 24 (9), 094301–094306, DOI: 10.1088/1674-1056/24/9/094301.

[9] KLOTZ A.R., HYNYNEN K., *Simulations of the Devin and Zudin modified Rayleigh-Plesset equations to model bubble dynamics in a tube*, Technical Acoustics., 2010, 30 (6).

[10] KOBIELARZ M., *Effect of collagen fibres and elastic lamellae content on the mechanical behaviour of abdominal aortic aneurysms*, Acta Bioeng. Biomech., 2020, 22 (3), 69–74, DOI: 10.37190/ABB-01580-2020-02.

[11] KOSHIYAMA K., WADA S., *Molecular dynamics simulations of pore formation dynamics during the rupture process of a phospholipid bilayer caused by high-speed equibiaxial stretching*, J. Biomech. 2011, 44(11), 2053–2058, DOI: 10.1016/j.jbiomech.2011.05.014.

[12] KRASOVITSKI B., KIMMEL E., *Shear stress induced by a gas bubble pulsating in an ultrasonic field near a wall*, IEEE Trans. Ultrason. Ferroelectr. Freq. Control., 2004, 51 (8), 973–979, DOI: 10.1109/TUFFC.2004.1324401.

[13] LI W., YUAN T., XIA-SHENG G., DI X., DONG Z., *Microstreaming velocity field and shear stress created by an oscillating encapsulated microbubble near a cell membrane*, Chin. Phys. B., 2014, 23, 124302, DOI: 10.1088/1674-1056/23/12/124302.

[14] LIN S.J., JAN K.M., WEINBAUM S., CHIEN S., *Transendothelial transport of low density lipoprotein in association with cell mitosis in rat aorta*, Arteriosclerosis, 1989, 9 (2), 230–236, DOI: 10.1161/01.ATV.9.2.230.

[15] MAN V.H., TRUONG P.M., LI M.S., WANG J., VAN-OANH N.T., DERREUMAUX P., NGUYEN P.H., *Molecular Mechanism of the Cell Membrane Pore Formation Induced by Bubble Stable Cavitation*, J. Phys. Chem. B., 2019, 123 (1), 71–78, DOI: 10.1021/acs.jpcb.8b09391.

[16] MIAO H., GRACEWSKI S.M., DALECKI D., *Ultrasonic excitation of a bubble inside a deformable tube: implications for ultrasonically induced hemorrhage*, J. Acoust. Soc. Am., 2008, 124 (4), 2374–2384, DOI: 10.1121/1.2967488.

[17] MILLER D.L., QUDDUS J., *Diagnostic ultrasound activation of contrast agent gas bodies induces capillary rupture in mice*, Proc. Natl. Acad. Sci. U.S.A., 2000, 97 (18), 10179–10184, DOI: 10.7863/jum.2002.21.12.1435.

[18] MILLER M.W., *Cell size relations for sonolysis*, Ultrasound. Med. Biol., 2004, 30 (10), 1263–1267, DOI: 10.1016/j.ultrasmedbio.2004.07.005.

[19] OLGAC U., KURTCUOGLU V., POULIKAKOS D., *Computational modeling of coupled blood-wall mass transport of LDL: effects of local wall shear stress*, Am. J. Physiol. Heart. Circ. Physiol., 2008, 294 (2), H909–919, DOI: 10.1152/ajpheart.01082.2007.

[20] PERENO V., LEI J., CARUGO D., STRIDE E., *Microstreaming inside Model Cells Induced by Ultrasound and Microbubbles*, 2020, 36 (23), 6388–6398, DOI: 10.1021/acs.langmuir.0c00536.

[21] QIN S., FERRARA K.W., *The natural frequency of nonlinear oscillation of ultrasound contrast agents in microvessels*, Ultrasound Med. Biol., 2007, 33 (7), 1140–1148, DOI: 10.1016/j.ultrasmedbio.2006.12.009.

[22] RAMIAR A., LARIMI M.M., RANJBAR A.A., *Investigation of blood flow rheology using Second-Grade viscoelastic model (Phan–Thien–Tanner) within carotid artery*, Acta Bioeng. Biomech., 2017, 19 (3), 27–14. DOI: 10.5277//ABB-00775-2016-05.

[23] ROWE A.J., FINLAY H.M., CANHAM P.B., *Collagen biomechanics in cerebral arteries and bifurcations assessed by polarizing microscopy*, J. Vasc. Res., 2003, 40 (4), 406–415, DOI: 10.1159/000072831.

[24] SASSAROLI E., HYNYNEN K., *Resonance frequency of microbubbles in small blood vessels: a numerical study*, Phys. Med. Biol., 2005, 50 (22), 5293–5305, DOI: 10.1088/0031-9155/50/22/006.

[25] SIERRA C., ACOSTA C., CHEN C., WU S.Y., KARAKATSANI M.E., BERNAL M., KONOFAGOU E.E., *Lipid microbubbles as a vehicle for targeted drug delivery using focused ultrasound-induced blood-brain barrier opening*, J. Cereb. Blood. Flow. Metab., 2017, 37 (4), 1236–1250, DOI: 10.1177/0271678X16652630.

[26] SNOWHILL P.B., SILVER F.H., *A Mechanical Model of Porcine Vascular Tissues-Part II: Stress-Strain and Mechanical Properties of Juvenile Porcine Blood Vessels*, Cardiovascular Engineering, 2005, 5 (4), 157–169, DOI: 10.1007/s10558-005-9070-1.

[27] STIEGER S.M., CASKEY C.F., ADAMSON R.H., QIN S., CURRY F.R., WISNER E.R., FERRARA K.W., *Enhancement of vascular permeability with low-frequency contrast-enhanced ultrasound in the chorioallantoic membrane model*, Radiology, 2007, 243 (1), 112–121, DOI: 10.1148/radiol.2431060167.

[28] WU J., *Theoretical study on shear stress generated by microstreaming surrounding contrast agents attached to living cells*, Ultrasound. Med. Biol., 2002, 28 (1), 125–129, DOI: 10.1016/S0301-5629(01)00497-5.

[29] YE T., BULL J.L. *Microbubble expansion in a flexible tube*, J. Biomech. Eng., 2006, 128 (4), 554–563, DOI: 10.1115/1.2206200.

[30] YU H., CHEN S., *A model to calculate microstreaming-shear stress generated by oscillating microbubbles on the cell membrane in sonoporation*, Biomed. Mater. Eng., 2014, 24 (1), 861–868, DOI: 10.3233/BME-130878.

Appendix A.
Program flowchart design

Supplementary illustrates the computational flowchart adopted in the present study, based on which we built the program on the COMSOL platform:

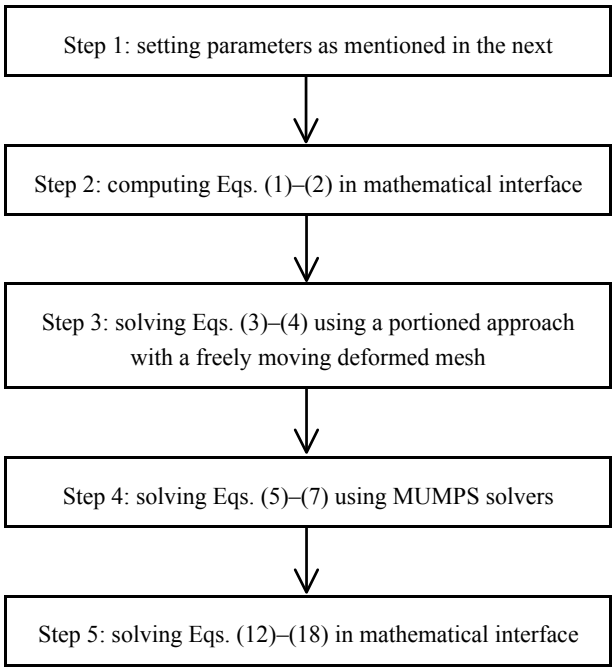

It should be noted that the system of governing equations along with initial and boundary conditions are solved using MUMPS and GMRES solvers, respectively.